Aerial photogrammetry to characterise and numerically model an ice jam in Southern Quebec

Jason Duguay [a,*], Karl-Erich Lindenschmidt [b], Mélanie Trudel[a] and Antoine Pruneau[a]

[a] Department of Civil Engineering, Université de Sherbrooke, 2500 boul. de l'Université, Sherbrooke, QC, Canada
[b] Global Institute for Water Security, School of Environment and Sustainability, University of Saskatchewan, 11 Innovation Boulevard, Saskatoon, Saskatchewan S7N 3H5, Canada
*Corresponding author. E-mail: jason.duguay@usherbrooke.ca

JD, 0000-0002-9600-3999; K-EL, 0000-0001-6348-2295

ABSTRACT

Collecting data on the dynamic breakup of a river's ice cover is a notoriously difficult task. However, such data are necessary to reconstruct the events leading to the formation of ice jams and calibrate numerical ice jam models. Photogrammetry using images from remotely piloted aircraft (RPA) is a cost-effective and rapid technique to produce large-scale orthomosaics and digital elevation maps (DEMs) of an ice jam. Herein, we apply RPA photogrammetry to document an ice jam that formed on a river in southern Quebec in the winter of 2022. Composite orthomosaics of the 2-km ice jam provided evidence of overbanking flow, hinge cracks near the banks and lengthy longitudinal stress cracks in the ice jam caused by sagging as the flow abated. DEMs helped identify zones where the ice rubble was grounded to the bed, thus allowing ice jam thickness estimates to be made in these locations. The datasets were then used to calibrate a one-dimensional numerical model of the ice jam. The model will be used in subsequent work to assess the risk of ice interacting with the superstructure of a low-level bridge in the reach and assess the likelihood of ice jam flooding of nearby residences.

Key words: ice-jam, numerical modeling, photogrammetry, remotely piloted aircraft, remote sensing, river ice

HIGHLIGHTS

- Photogrammetry datasets useful for calibrating 1D numerical river ice jam models.
- Remotely sensed digital elevation models of grounded ice can provide estimates of ice jam thickness.
- Remotely sensed large-scale orthomosaics provide insights into ice jam formation and evolution.

1. INTRODUCTION

Ice rubble hitting the superstructure of a low-level bridge can compromise its structural integrity. For example, on January 12, 2018 an ice run near Sherbrooke, Quebec, Canada, destroyed a low-level railway bridge and a nearby footbridge. The run also caused a brief ice jam that resulted in the St Francois River unprecedentedly rising by 2 m in less than 45 min (Béland 2018). Selecting the elevation of low-level bridges to avoid, or at least reduce, the damage caused by rapidly forming ice runs and ice jams requires a full understanding of the hydrogeomorphologic and cryologic characteristics of the reach. Numerical fluvial ice models can help in this regard if validation measurements such as water and ice elevation profiles, discharges, and ice volume estimates of the event are available (Carson *et al.* 2011; Lindenschmidt 2017; Blackburn & She 2019). However, the unpredictability of most dynamic ice events usually makes gathering such data difficult. Recently, remotely piloted air-crafts (RPAs) have allowed geoscience researchers to obtain detailed digital elevation models (DEMs) of their subjects using aerial structure from motion (SfM) photogrammetry (Westoby *et al.* 2012; Ely *et al.* 2017; Albadra *et al.* 2020; David *et al.* 2021). The technique generates high-resolution DEMs of an area of interest, such as an ice jam, from overlapping aerial photographs taken during a short flight. Most commercial photogrammetry software also generate high-resolution coloured orthomosaics of the area, which provide a useful tool to assess ice jams at full scale and gain insights into how they formed.

At the spatial scale of an ice jam, aerial photogrammetry can provide advantages over other remote sensing techniques. For one, a team can be dispatched to fly at specified time intervals as the ice jam evolves. This is not possible for satellite-based radar and optical remote sensing systems, whose temporal resolutions are determined by the orbit of the satellite (Los & Pawlowski 2017; Zhang et al. 2019). Furthermore, a single RPA photogrammetry flight can produce a DEM and an orthomosaic of the ice jam with ground resolutions on the order of 1–5 cm (Alfredsen et al. 2018), thus providing far greater detail than satellite remote sensing systems, whose spatial resolutions are of the order 10–100 m (Los & Pawlowski 2017; Lindenschmidt & Li 2018). Also, the low altitude of the RPA (typically 50–100 m above the river's water level) means the camera is generally unaffected by cloud cover, which is often an issue with satellite-based optical sensors (Tracy & Daly 2003; Unterschultz et al. 2009; Chu & Lindenschmidt 2016). Exceptionally, light detection and ranging systems (LiDAR) can also provide high-resolution DEMs and orthomosaics (if equipped with a mapping camera), yet at 1- to 2-order-of-magnitude greater cost than popular photogrammetry RPAs. Finally, by using a light-weight RPA, such as DJI's Mavic 3 Mini, which weighs less than 250 g, many regulatory flight constraints imposed by transport agencies are not applicable thus simplifying flight logistics over ice jams in densely populated regions.

Despite these advantages, RPA photogrammetry has received little attention in the study of fluvial ice processes. Alfredsen et al. (2018) used the technique to extract 2D elevations and characterise ice type information of an ice jam and estimate the thickness of the ice by subtracting a measured bathymetry from the photogrammetrically derived DEM of grounded ice sections. They also used the orthomosaics to identify key features of the ice jam's formation. Rødtang et al. (2021) used DEMs derived from RPA photogrammetry to estimate ice thicknesses and volumes on a steep reach of river in Norway prone to forming complex successions of anchor ice jams. The technique proved adequate for measuring ice thicknesses and elevations over hard, or impossible, to access alpine reaches in difficult terrain. Ehrman et al. (2021) quantified the roughness of various intact ice covers using DEMs generated by RPA photogrammetry and used statistical techniques to distinguish between smooth and rough ice types. Ehrman et al. (2021)'s roughness estimates were used to predict the Manning's roughness coefficient of the underside of the ice cover. These studies have shown the promise of RPA photogrammetry for documenting fluvial ice processes such as ice jams, yet its potential to assist in numerical modelling of ice jams has yet to be assessed.

Numerical fluvial ice models have been used most notably to predict ice jam flood hazards and risks (Das et al. 2020; Das & Lindenschmidt 2021), select the height of dikes (Lindenschmidt & Rokaya 2019), forecast ice jam water levels (Williams et al. 2021; Das et al. 2022), and assess how in-stream infrastructure such as low-level bridges are affected by ice jams (Daly & Vuyovich 2003; Zufelt 2005). High water levels are frequently used to calibrate numerical ice models. In many cases, such data can be derived from photographs (Lindenschmidt et al. 2012), pressure transducers placed preemptively in locations prone to dynamic breakups (Beltaos 2019), or surveys along the bank of an ice jam after it has set in place (Beltaos 2018; Rokaya et al. 2019). However, these methods generally provide sparse information on ice jam elevations and are prone to miss relevant topological information. For example, as discharge recedes after the formation of an ice jam, rubble ice may ground on gravel bars near the banks (Alfredsen et al. 2018), while sinking lower into the thalweg in others, causing an unequal lateral ice elevation profile to develop. Also, as rubble ice enters bends and meanders, it can force the outer sections of the ice jam higher, resulting in an elevated shear wall compared to the surrounding ice (Beltaos & Burrell 2010). Furthermore, large boulders and obstructions in the river may force ice rubble to flow around them, causing one side of the ice to heave upwards resulting in significant lateral elevation variations. Accounting for spatial variability is good practice to accurately calibrate a numerical ice jam model or reconstruct the events leading to the jam's formation. Despite its importance, this variability has frequently been overlooked, likely in part due to a lack of a low-cost and easily deployable technique to obtain high-resolution elevation maps of the ice jam.

In this study, we use DEMs and orthomosaics obtained from RPA photogrammetry to study an ice jam that formed on the Aux Saumons River in the province of Quebec, Canada in 2022. The datasets are also used to calibrate a 1D numerical fluvial ice model, specifically by using the ice elevation DEM to calibrate the ice elevations predicted in the numerical model. The model will be used in subsequent work to assess the likelihood of ice interacting with a low-level railway bridge on the reach and develop an ice jam flood hazard map for nearby residences. The strengths and weaknesses of the RPA photogrammetry datasets are examined, and practices are suggested to increase the quality of RPA photogrammetry datasets for calibrating and validating numerical ice models. Our findings are of interest to those involved in documenting and numerically assessing the hazards posed by ice jams to riverine communities in northern climates.

2. STUDY SITE AND METHODS

2.1. Study site and ice jam description

On February 18, 2022, a 2.05-km long ice jam formed on the Aux Saumons River near the town of Huntingville in the province of Quebec, Canada. The reach containing the ice jam is just upstream of the confluence the Aux Saumons River makes with the Massawippi River. The Aux Saumons' watershed area is 488 km^2 and the river has an average discharge of 9 m^3/s, a maximum recorded discharge of 251 m^3/s, an average slope of 0.48% and an average depth and width of ≈1.4 and ≈30 m, respectively. The ice jam extended from the confluence to a run-of-the-river dam near the town of Huntingville. The location and extents of the ice jam are shown in Figure 1. Downstream of the dam, a road bridge, a railway bridge, and a foot bridge cross the river. The bathymetry of the Aux Saumons River along the ice jam was manually surveyed by a team in 2019 for a different project. A total of 15 cross-sections were surveyed downstream of the dam with an average longitudinal spacing of 40 m.

2.2. Discharges and water levels

Since 2021, two water level probes have been available in the study area: the probe at the hydrometric station, which is located in the ice jam, and another located just upstream of the dam (and hence upstream of the ice jam). The maximum water level at the probe in the ice jam was attained on February 18, 2022 at 9:45 a.m., compared to 45 min later at 10:30 a.m. for the probe upstream of the dam. Photos taken upstream of the dam show the ice cover to have completely given way after the formation of the ice jam on February 18, 2022, meaning the dam's water level measurements were for open water and, therefore, can be used to estimate the discharge using the weir equation over the run-of-the-river dam. The
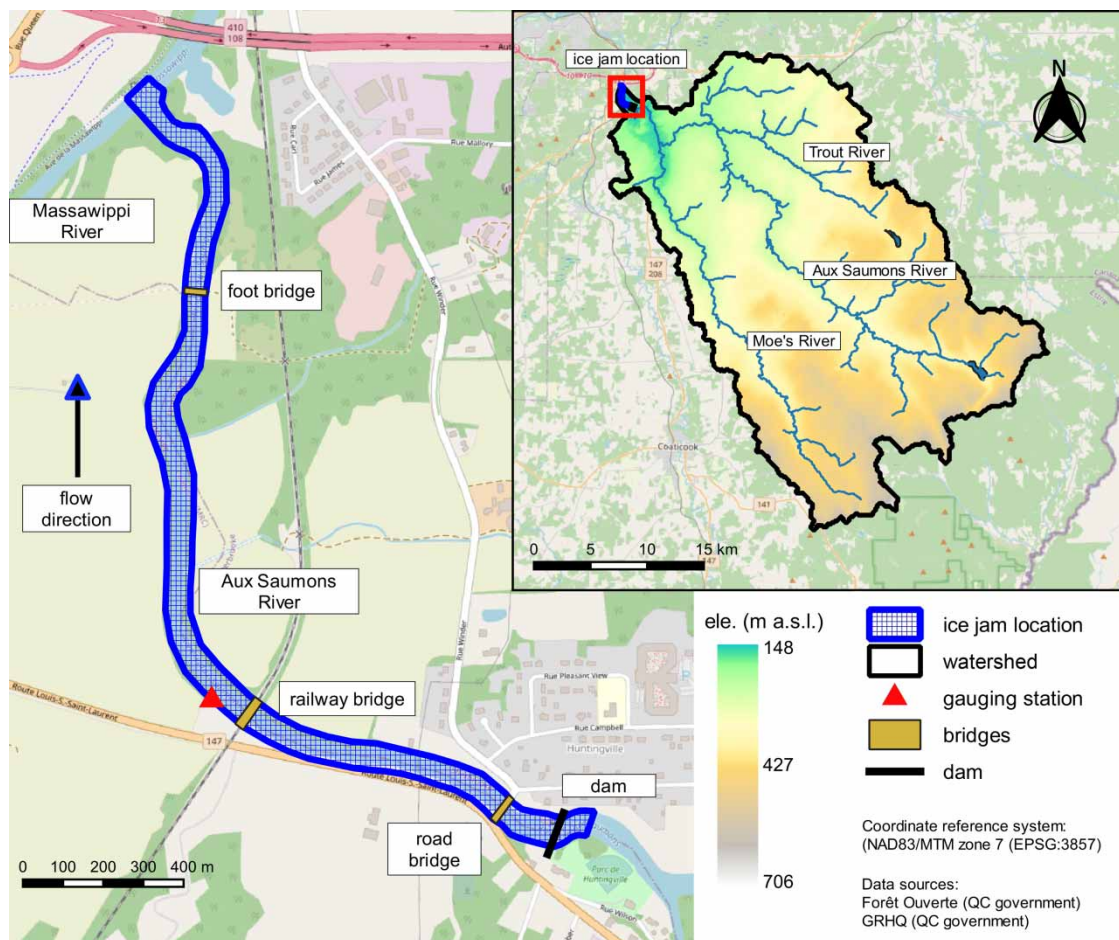

Figure 1 | Details of the Aux Saumons River 2022 ice jam. The longitudinal extent of the ice jam is depicted by the blue-hashed polygon above the Aux Saumons River. Flow is from south to north.

standard weir equation was used with the calibrated HEC-RAS model to obtain the discharge measurements based on water surface levels. The weir coefficient (0.6) was determined using the open water discharge measurements from the provincially operated station 750 m downstream from the dam. The discharge in the day following the formation of the ice jam varied between 38 and 52 m³/s and then decreased to 11 m³/s on February 21 when the RPA flights were performed. The discharge estimates based on the weir equation over the run-of-the-river dam and the corresponding water surface levels at the gauge within the ice jam and at the dam are presented in Figure 2.

2.3. Meteorological events causing the ice jam

A rain on snow event on February 17, 2022 caused excessive snow-melt run-off and a rapid rise in the Aux Saumons River's water level. Between 28 and 35 mm of rain were recorded at numerous weather stations in the region around the Aux Saumons' watershed on February 17, a day prior to the formation of the ice jam on February 18. This initiated the dynamic breakup of the ice cover and ultimately the ice jam downstream of the dam on the Aux Saumons River. Because the precipitation event happened mid-winter, the ice cover on the Aux Saumons was intact and structurally competent with no thermal degradation prior to the formation of the ice jam. After the formation of the ice jam, the air temperature dropped down to between −5 and −15 °C until February 22, when air temperatures rose above zero again to 6.5 °C. A total of 15 mm of rain was recorded on February 22 and was responsible for a rapid rise in the water level observed at the gauging station between 21 and 22 February (see Figure 2(b)).

2.4. Photogrammetry acquisition and processing

On February 21, 2022, two photogrammetry flights were performed using a remotely piloted DJI Mavic Pro 2 aerial RPA. The RPA is equipped with a global navigation satellite system (GNSS) using GPS/GLONASS for positioning and a colour camera with a resolution of 3,840 × 2,160 pixels. The RPA was flown on a preplanned flight grid with the camera pointing downward in the nadir position. The first flight extended 650 m upstream of the railway bridge to the dam and collected 638 images, whereas the second flight went 1,500 m downstream of the railway bridge to the confluence and collected 829 images. The flight upstream was composed of five flight lines while the downstream flight had four. The flights were programmed in the flight planning software DroneLink to have a sufficient overlap between the images for accurate post-processing (a least 75% lateral and longitudinal overlap).
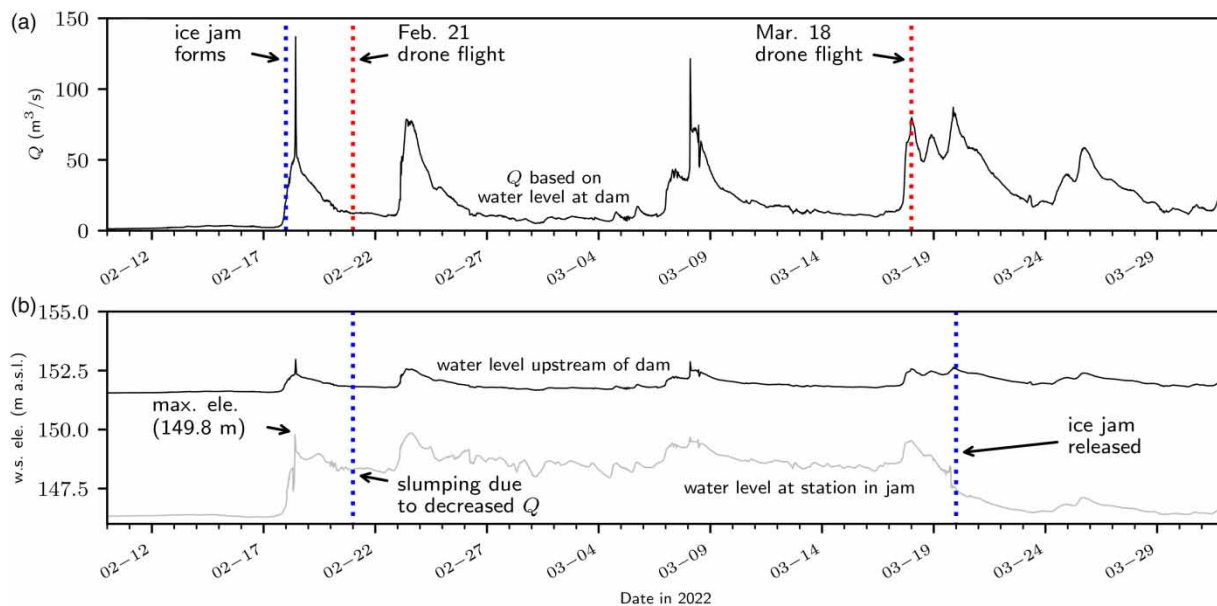

Figure 2 | (a) Time-series of instantaneous discharge in the Aux Saumons River (Q_{AS}) estimated from water levels measured at the probe upstream of the dam. The first set of photogrammetry data was surveyed on 21 February and the second on 18 March prior to its full release on the 20 of March 2022. (b) Fluctuations in the instantaneous water surface elevations both upstream of the dam, and at a point within the ice jam, caused by the onset of the ice jam and subsequent fluctuations in the Aux Saumons River's discharge. Red diamond indicates the maximum instantaneous water surface elevation of 149.8 m registered at the station on February 18 when the ice jam formed.

For the upstream flight, six ground control points (GCPs) were placed on, or near the railway bridge, and another GCP was placed near the road bridge upstream. The downstream flight only had four GCPs on the foot bridge and two GCPs near the railway bridge. The coordinates of the GCPs were taken using a GNSS-RTK receiver with a precision of ± 2 cm. On March 18, 2022 a single flight was performed over the section between the railway bridge prior to the jam's release on March 20, 2022. No GCPs were placed during this flight as it was originally intended to obtain an orthomosaic to visually assess the degradation of the ice jam.

The photos from both dates were processed in the commercial photogrammetry software Pix4D version 4.6.3. The software uses a Structure from Motion (SfM) algorithm to create a three-dimensional point cloud of the ground's elevation and notable landmarks such as bridges or dams. The point cloud was used to derive a DEM with a spatial resolution of 5 cm. A coloured high-resolution (0.7 cm per pixel) orthomosaic of the entire flight zone was also output from Pix4D.

During processing, the GCPs were used to georeference the DEMs and orthomosaics of the flights of February 21, 2022. The root-mean-squared error (RMSE) values of the targets visible in the orthomosaics from their measured locations using the GNSS were both 0.02 and 0.02 m in the lateral and longitudinal directions, respectively. The RMSE between the elevations obtained from the DEM and the measured GNSS elevations was 0.02 m in the upstream portion. The RMSE values were similar for the downstream flight, however the DEM was found to be artificially bowed which introduced important errors in the elevations of the flood plains compared to a provincial LiDAR database. For this reason, only the upstream DEM is considered to have valid elevations to be used in any further analysis. The upstream DEM of February 21, 2022 was validated against the provincial LiDAR dataset in addition to the GNSS measurements of the GCPs. The vertical offsets between DEM and LiDAR were less than 30 cm on the flood plains and often less than 10 cm on hard features such as the adjacent road and bridges.

2.5. HEC-RAS ice modelling description

HEC-RAS is a popular 1D–2D numerical model developed by the United State's Army Corps of Engineers to model free surface channel flows. However, it can also model the effect of static ice covers and wide-river ice jams (equilibrium ice jams) on a channel's hydraulics in 1D only. For reaches of gradually varied open-channel flow, the energy equation is used at each cross-section to obtain an estimate of the river's water surface level. At sections containing rapidly varied flow (e.g. hydraulic jumps, contractions, expansions, ice jams) HEC-RAS instead solves the momentum equation to estimate the water surface level. The momentum equation accounts for how forces acting on a control volume between two cross-sections alter the momentum of the fluid within it. The forces acting on the control volume are the hydrostatic pressure forces, the gravitational force and the frictional forces acting on the control volume (i.e. shear stress on the bed). Both the energy and momentum equations are modified to account for the effects that a static ice cover or an equilibrium ice jam have on water surface levels.

When simulating a static ice cover, in addition to discharge and boundary conditions, the user must also specify; (1) the cross-sections between which the ice cover is present, (2) the thickness of the ice at each cross-section, (3) the ice cover's roughness, and (4) its specific gravity. The discharge of an ice-covered channel (Q) is estimated using Manning's equation:

$$Q = \frac{1.486}{n_c} A_i R_i^{2/3} \tag{1}$$

where n_c is the composite roughness of the ice-covered channel section calculated using the Belokon-Sabaneev formula (Equation (2)), A_i is the available flow area (m^2) and R_i (m) is the hydraulic radius of the ice-covered channel. The Manning's roughness of the bed (n_b) is the same as that of the open-channel's and the Manning's roughness of the underside of the ice n_i can vary from 0.008 to 0.06 depending on the type of ice constituting the ice cover (see Tables 11-1 of US Army Corps of Engineers, 2021).

$$n_c = \left(\frac{n_b^{3/2} + n_i^{3/2}}{2} \right)^{2/3} \tag{2}$$

The wide-river ice jam functionality of HEC-RAS allows the user to predict the thickness of an ice jam that would form between any two cross-sections and the effect this jam would have on water levels. The model predicts the thickness (t, m) of the jam at each section by equating the forces preventing the ice jam from moving downstream to the forces attempting

to dislodge it. Equation (3) is the ice jam force balance equation used in HEC-RAS. The two external forces acting on the ice jam in Equation (3) are its weight in the downstream direction ($\rho'gS_w$ term, where ρ' is the ice's density (kg/m^3), g is the acceleration of gravity, S_w is the water surface slope (m/m)) and the shear stress on the ice jam's underside due to skin-drag caused by flowing water (τ_i, N/m^2). For the ice jam to be in equilibrium, the forces due to weight and skin-friction are resisted by the shear stress along the banks and the longitudinal stresses in the ice cover $\bar{\sigma}_x$. The resistive stress terms in Equation (3) ($d\bar{\sigma}_x t/dx$, $2\tau_b t/B$, where τ_b is the shear resistance of the two banks) are both a function of t. The wide-ice jam model adjusts t to equate the acting and resistive forces, resulting in the thickness and water surface profiles of the ice jam. Interested readers can find a more complete description of HEC-RAS's wide-ice jam model in U.S. Army Corps of Engineers (2022).

$$\frac{d(\bar{\sigma}_x t)}{dx} + \frac{2\tau_b t}{B} = \rho'gS_w t + \tau_i \tag{3}$$

For ice jam simulations, HEC-RAS assumes steady-flow conditions, which is a limitation of the model. In addition, the model is sensitive to the distance between sections, which can lead to instabilities (Beltaos & Tang 2013). The latest versions of HEC-RAS can interpolate bathymetric sections to create a 2D surface, making it easier to add interpolated sections to ensure model stability.

When simulating a wide-river ice jam, in addition to discharge and boundary conditions, the user must specify (1) the location and ice thickness of the toe and head of the ice jam, (2) Manning coefficient of the ice, which can be estimated according to depth and the ice thickness by HEC-RAS using the equation of Nezhikhovsky (1964), (3) ice parameters including the porosity of the rubble comprising the jam, usually taken as 0.4 and the ratio of the lateral-to-longitudinal internal stresses within the rubble mass (K_1) usually taken as 0.33, (4) the maximum allowable flow velocity underneath the jam (V_{max}) with default value of 1.5 m/s, yet recommended to be higher by Beltaos & Tang 2013, and (5) the internal friction angle of the rubble comprising the jam (φ) with default value of 45°, but can be varied to calibrate the simulation (Beltaos & Tang 2013; Beltaos 2018, 2019).

2.6. Proposed method to calibrate a fluvial ice model with photogrammetry DEMs

Conventionally, the internal friction angle and the ice thickness at the toe and head of an ice jam can be adjusted according to observed elevations, usually taken at hydrometric stations at a few locations within the ice jam. The sparsity of observations limits the quality of the calibration. However, elevations extracted from a photogrammetry DEM provide much greater resolution, but are generally acquired after the ice jam formed when the discharge was significantly lower. This highlights an important drawback with using photogrammetric DEMs to assist in the calibration of a numerical ice jam model – it is very difficult to perform an RPA flight at the time the ice jam forms, and because of decreasing discharges in the falling limb of the hydrograph, the resulting DEM will nearly always be an underestimate of the ice jam's top of ice profile during its formation. Thus, a method for calibrating ice parameters is proposed to use photogrammetry DEMs most effectively according to the following five steps:

1. Perform a wide-river ice jam model using the flow at the time of ice jam formation to obtain simulated ice thickness and elevation profiles.
2. Perform a static ice model using the flow at the time of photogrammetry acquisition using the ice thicknesses simulated in step 1.
3. Compare the static ice model's top of ice elevation profile with the photogrammetry DEM.
4. Redo step 1 after modifying φ and the thicknesses at the toe and the head of the ice jam and then repeat steps 2 and 3.
5. Iterate steps (1) through (4) until a satisfactory profile is obtained.

3. RESULTS

3.1. Ice jam description using orthomosaic images

The orthomosaics provide insights into the formation and state of the ice jam. For one, the merged orthomosaic from February 21 shows the ice jam stretched from the confluence to the dam over a length of ≈2.05 km (Figure 3(a)). The width of the ice jam is approximately 35 m, but attained up to 50 m in some sections. The ice jam contains many large blocks of ice within the confluence downstream and in the first 200 m upstream into the Aux Saumons River (see Figure 3(b)). Further upstream, larger blocks of ice are no longer apparent. The ice jam has a rough texture upstream of the confluence to within
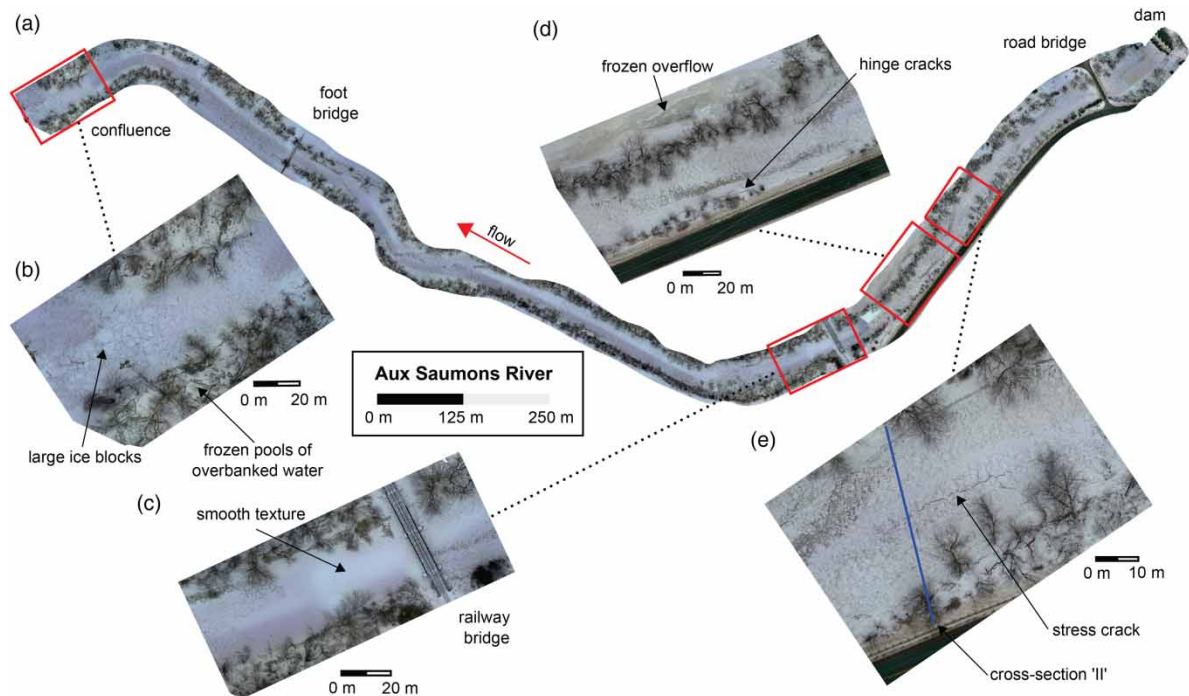
Figure 3 | Important features of the ice jam visible in the composite orthomosaic of the Aux Saumons River of February 21, 2022. (a) Entire extent of the ice jam on the Aux Saumons River between its confluence with the Massawippi River downstream and the dam upstream. (b) Examples of large blocks of horizontally orientated ice near and within the confluence. (c) Smooth and rough texture downstream and upstream of the constriction of the railway bridge. (d) Evidence of frozen flood waters and hinge cracks near the banks. (e) Longitudinal stress crack between grounded ice near the right bank and slumped ice near the right bank.

≈78 m of the railway bridge. However, near the railway bridge the ice takes on a visually smoother texture than the rest of the ice jam (Figure 3(c)). Upstream of the railway bridge, the ice jam again adopts the rougher texture. Deep hinge cracks are visible along the banks at many locations along the ice jam (Figure 3(d)). Frozen pools of overbanked flood waters are also visible at many locations, but especially near the confluence up to the first bend. Upstream of the railway bridge, a long and narrow pool of frozen overbanked water is visible near the right bank (Figure 3(d)). This pool likely formed due to overbanking of water when the ice jam formed near the railway bridge. Longitudinal cracks are also visible along the ice cover (Figure 3(e)) and are likely due to vertical shear stresses caused by one side of the ice jam slumping while the other was supported by the bed of the river as the discharge receded after February 18, 2022.

3.1.1. Ice thickness estimates

Inspection of the upstream DEM for February 21 shows a number of zones in the ice jam with locally higher elevations compared to the surrounding ice. Four such zones are identified in Figure 4(a). The humped surface close to the left bank on cross-section II in Figure 4(a) is a good example, with a raised section of ice near the left bank and a slumped section near the right bank. Between the humped and the slumped section, a prominent longitudinal crack is visible at the cross-section's mid-length (see II in Figure 4(b)).

As the discharge receded in the days after the ice jam formed on February 18 (from 38 to 11 m³/s), the water surface elevation at the gauging station dropped by ≈1.4 m from a peak of 149.8 m recorded on February 18 to the elevation of 148.4 m recorded on February 21 (see Figure 2). When this happened, the ice to the right slumped lower into the deeper thalweg, and the ice to the left grounded on the bed at cross-section II. This created sufficient vertical shear and bending stresses in the ice jam to form the longitudinal crack. Further evidence that the ice jam descended is noted by the elevated regions of ice left higher along the banks in the DEMs at numerous locations after the central portion of the ice jam descended lower. Long hinge cracks along the banks visible in the orthomosaic of February 21 also provide evidence of the central section of the ice jam slumping lower as the discharge receded. Also, the same blocks of ice and woody debris to the left of the crack in the February 21 orthophoto are still visible in the March 18 orthophoto (Figure 4(d)). However, a preferential flow channel
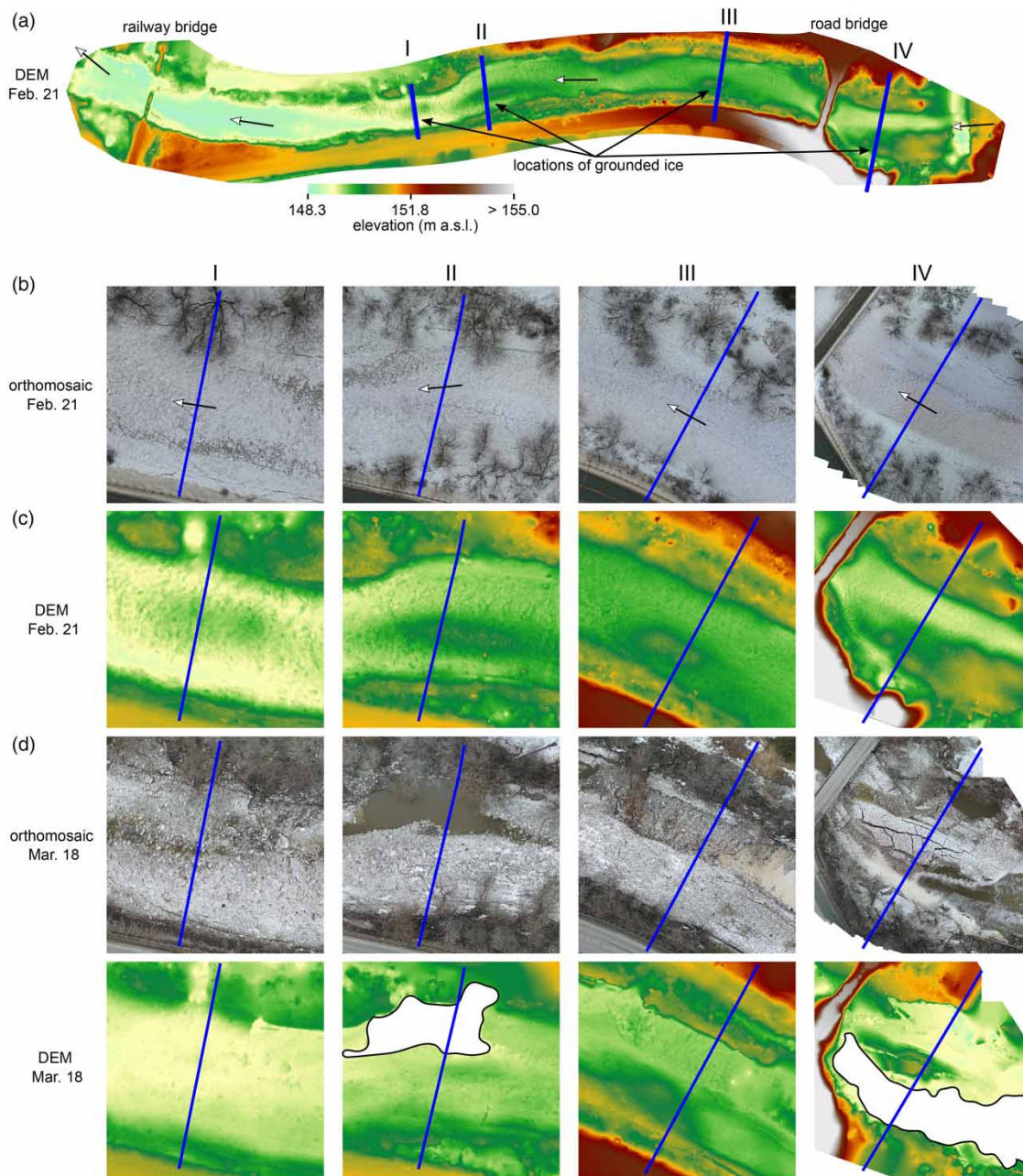
Figure 4 | Surface ice elevations and orthomosaics of the Aux Saumons River upstream of the railway bridge derived from RPA photogrammetry on February 21, 2022. (a) Cross-sections over humps of locally elevated ice are indicated by roman numerals I–IV. (b) February 21 orthomosaic close-ups for each cross-section. (c) February 21 DEM close-ups for each cross-section. (d) March 18 orthomosaic close-ups for each cross-section. (e) March 18 DEM close-ups for each cross-section. White filled polygons delineate erroneous regions in the DEM caused by open water.

through the ice near the right bank thermally and mechanically degraded the ice there, explaining why open water is visible in this location of the March 18 orthomosaic. The fact that the same pieces of ice rubble and woody debris are present in the orthophotos on both dates provides evidence that the ice jam was grounded on the bed in these locations, which prevented it from being degraded by active flow.

Ice elevation profiles along each cross-section are presented in Figure 5. The bathymetric profiles measured in 2019 are also provided. Focusing first on cross-section II in Figure 5(b), we can clearly see the hump closer to the left bank and the slumping near the right bank as measured in the February 21 DEM. The hump is located above the thalweg of the 2019 bathymetry,
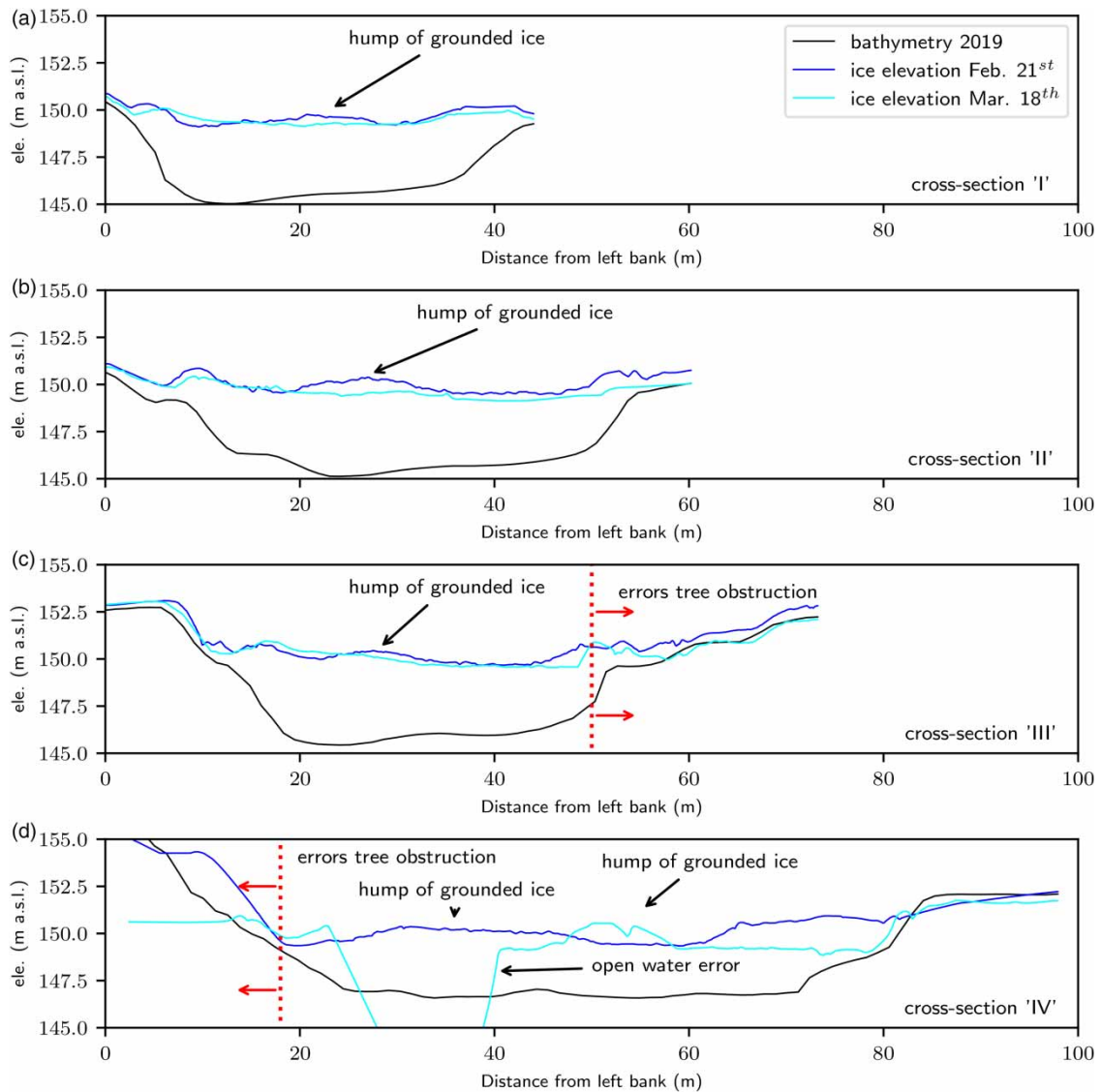
Figure 5 | Lateral ice surface elevation profiles at cross-sections I–IV obtained from DEMs of 21 February and 18 March, 2022. Bathymetric profiles interpolated from the 2019 survey are also presented. The locations of each cross-section are depicted in Figure 4.

however, it is possible the thalweg has shifted to the right since. Regardless, if an average bed elevation of 145.7 m is considered at cross-section II, the thickness of the ice in the humped section can be estimated to be ≈4.2 m by subtracting 145.7 from 149.9 m. Following a similar approach at cross-sections I, III, and IV gives ice thickness estimates of 4.0, 4.2, and 3.4 m, respectively, at these locations. Irregularities in the bed elevation profiles may have introduced some uncertainty in the estimated values of ice thickness on the order of ≈± 0.25 m.

The orthomosaic from March 18 for section IV shows evidence of longitudinal and lateral cracking consistent with ice grounded on the rocky riffle section downstream of the dam (see Figures 4(d) and 6). The lateral elevation profile from the March 18 DEM in Figure 5(d) shows an erroneous elevation profile between 22 and 40 m from the left bank, followed by an irregular 20 m wide profile corresponding to the cracked grounded ice, before another section of mixed ice and open water near the right bank.

We have used information available in the orthomosaic (i.e. cracking) and in the DEM (i.e. locally raised sections near the banks and raised sections on shallow bathymetry) of February 21, 2022 as compelling evidence of grounded sections of ice along the ice jam. However, due to a number of practical constraints, including safety considerations, lack of trained personal and difficulties measuring the thickness of a nearly 4-m thick ice jam, it was not possible for us to go out on the ice jam to

measure its thickness. Future efforts might benefit from ground penetrating radar to measure the ice thickness or potentially using specialty drilling equipment capable of attaining depths on the order of 3–5 m. The effectiveness of such methods needs to be addressed in future work.

The ice surface elevations show some variations between the DEM of March 18 and that of February 21. On March 18, the ice jam elevation at the gauging station was 149.1 m at the time of the drone flight, ≈0.7 m higher than the elevation of 148.4 m measured during the February 21 flight (see Figure 2(a)). The rise in elevation likely corresponds to the ≈64 m^3/s rise in discharge between both dates (Q of 11 and 75 m^3/s on February 21 and March 18, respectively). Discrepancies between the DEMs and the bathymetry are apparent near the right bank of sections I, II, and III. These discrepancies are principally caused by tree branches, shrubs, and snow obscuring views of the ground as measured by surveyors and the provincial LiDAR DEM combined to make the bathymetry profiles. Exceptionally, section IV shows a considerable deviation between the DEM profiles and the bathymetry near the left bank. However, inspection of this location in Figure 6 indicates the discrepancies were the result of large trees present there.

3.2. Photogrammetry to calibrate a 1D HEC-RAS model of the ice jam

3.2.1. Model setup and open water calibration

A 1D HEC-RAS model of the reach downstream of the dam to the confluence was constructed. The bathymetry was constructed from 15 cross-sections along the reach measured during a recent, yet unrelated project. The cross-sections were interpolated following the thalweg to generate a 2D bathymetric surface. The bathymetry was combined with a provincial LiDAR DEM of the neighbouring floodplains. HEC-RAS cross-sections were defined at an interval of approximately 40 m. The modelled width of the reach varies between 30 and 40 m. Thus, the spacing between measured cross-sections is on the order of magnitude of the river's width as recommended by Beltaos *et al.* (2012) and Beltaos & Tang (2013). The reach includes two bridges (the railway bridge: A07078-1 and the road bridge: P-07078) and a dam (X0002636). These structures were surveyed with a real-time kinematic GNSS so their openings could be accurately included in the HEC-RAS model (see Figure 7).

The model was first calibrated for open water conditions using flow data measured with an acoustic Doppler current profiler (ADCP) upstream of the dam and water levels measured along the reach downstream of the dam with a GNSS. Data were acquired on March 21, 2020 (38.1 m^3/s) and March 26, 2021 (37.8 m^3/s) in the context of an entirely different project. The March 21, 2020 water level measurement was done with a GNSS on a kayak and provided a water level profile from the dam to the confluence. In contrast, only three water surface level points were taken on March 26, 2021.
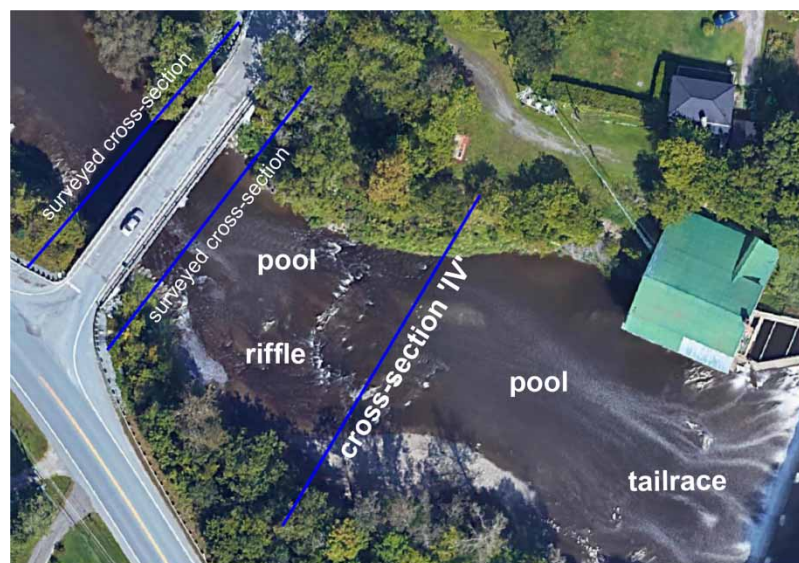

Figure 6 | Details of the flow and bathymetry upstream of the road bridge during the summer. A prominent riffle section is visible in the aerial image. Source: Google Earth.
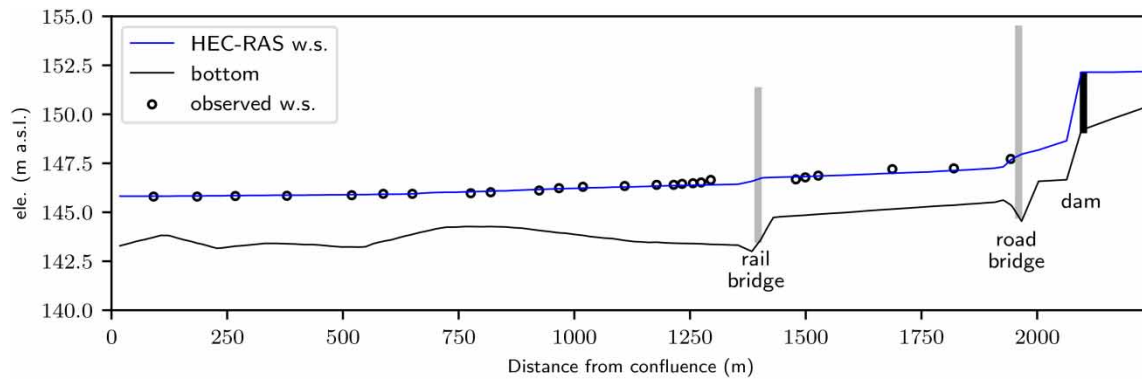
Figure 7 | Open water calibration of the 1D HEC-RAS model from the confluence up the dam in the town of Huntingville, Quebec. The solid blue line indicates the calibrated water surface level, whereas the circles indicate the observed water surface level profile as measured by GNSS. The black line indicates the bathymetry of the modelled reach. Bridges indicated by gray bars, dam indicated by the black bar.

A normal depth boundary condition was defined at the downstream end of the HEC-RAS model. The slope at the downstream boundary was adjusted to correspond to that of the normal depth in this location. Afterwards, a Manning's coefficient of 0.028 was determined to accurately reproduce the measured water surface profile over the first 600 m upstream of the confluence and a Manning's coefficient of 0.038 was used for the remainder of the reach. The slope set at the downstream boundary condition was 0.0001. Figure 7 shows the calibrated and observed levels for March 21, 2020.

3.2.2. Ice jam modelling

The model was calibrated according to the procedure described in subsection 2.6. The ice thickness estimate of 3.4 m was used as the first ice thickness estimate for the head of the ice jam. The model showed little sensitivity to ice thickness at the toe of the jam, and this value was estimated at 0.7 m. A φ value of 42° gave the best results. This value is lower than the HEC-RAS's default value. Beltaos & Tang 2013 obtained higher values for this parameter. However, the rivers studied were much wider than the Aux Saumons River, which could explain this difference.

Comparison with the water surface elevations at the time of ice jam formation on February 18, 2022 is more difficult, as the simulation is in steady-state mode with a discharge of 39 m^3/s, however the elevations varied from a maximum of 149.86 m at the gauging station to a nearly stable elevation of 149.05 m a few hours after the ice jam's formation. The simulated elevation at the gauging station when the ice jam formed was 149.83 m. Discharge (11 m^3/s) and elevations were much more stable on February 21, 2022, during the photogrammetry flight. The water surface elevation at the gauging station was 148.6 m and the simulated elevation was 148.4 m (Figure 8).

The simulated thicknesses at cross-sections I, II, III, and IV are, respectively, 4.18, 2.39, 2.83, and 1.0 m, respectively. The thicknesses measured from the photogrammetry DEM correspond at station I (4.0 m) but are higher at stations II (4.2 m), III (4.2 m), and IV (3.4 m). Higher simulated elevations are obtained at nearby sections. Uncertainties related to the bathymetry may also help explain the differences between the thicknesses estimated from the photogrammetry DEM and the simulated ice thicknesses using HEC-RAS. In general, the top of ice elevation profile extracted from the photogrammetric DEM aligns well with the predicted top of ice elevations of HEC-RAS (Figure 8(b)).

4. STUDY LIMITATIONS AND AREAS FOR IMPROVEMENT

4.1. Photogrammetry

Tree branches obscuring direct views of the ice jam limit the quality of the photogrammetrically derived DEM. Generally, a higher level of confidence can be placed in the elevations estimated in the center of the channel, yet much less so near the banks where the views of the ice are obstructed by tree branches. If elevations near the banks of the river are of special interest, then a RPA equipped with a LiDAR payload and a camera may be more appropriate. The high frequency LiDAR scan can provide detailed ground elevations even through thick vegetation (Bigdeli *et al.* 2018) and the photographs can be used to produce an orthomosaic and add colour to the LiDAR point cloud. However, a LiDAR-equipped enterprise-grade RPA is currently at least an order of magnitude more expensive than a consumer-grade RPA equipped with an optical camera suitable for performing photogrammetry.
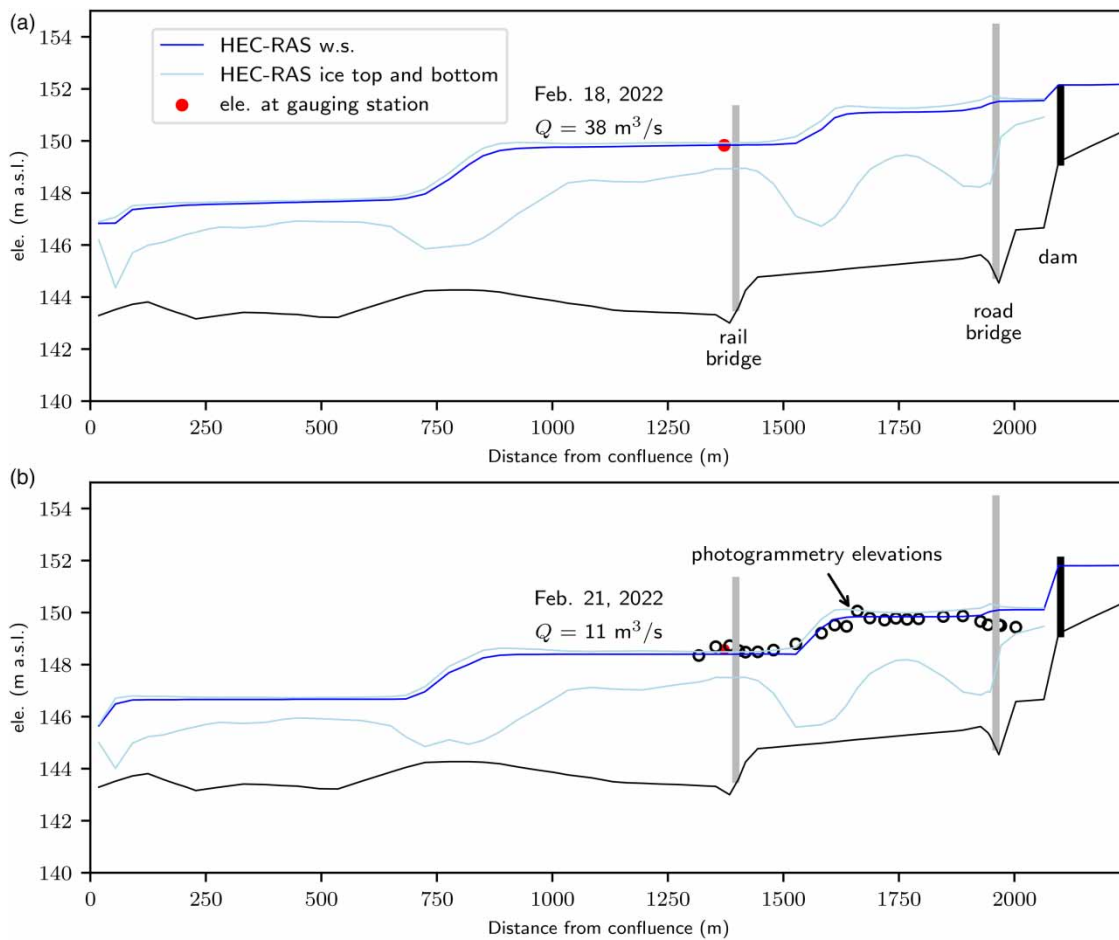
Figure 8 | (a) HEC-RAS wide-ice jam modelling results of the reach for the February 18, 2023 conditions. (b) HEC-RAS static ice cover model using the ice thickness profile from (a) but with the lower discharge on February 21, 2023. The water surface elevation at the gauging station (b) ≈1.25 m lower than that in (a) due to the ice jam slumping as the discharge decreased.

Placing ground reference points at regular spacings along the entire flight area is recommended to obtain the highest quality DEMs (Alfredsen *et al.* 2018; Kalacska *et al.* 2020). However, various constraints such as restricted access to private property, limited sunlight hours, large spatial scales involved, and limited access to the opposing shore, due either to the river itself, or the absence of a bridge can make placing sufficient ground reference points difficult. An RPA equipped with a real-time kinematic module (RTK) can be used to provide centimeter accurate geotagged locations of each image (Kalacska *et al.* 2020). An RTK-equipped RPA will likely considerably reduce the dependency on ground reference points (Kalacska *et al.* 2020), thus freeing time for personnel to perform flights over a larger area of the ice jam.

An improved DEM could have been attained for the purposes of calibrating a 1D numerical ice model if the RPA flight was performed on the February 18, 2022 immediately after the ice jam formed. This might have allowed the ice jam to be modelled in a single step using the wide-river ice jam module of HEC-RAS, instead of the iterative process described in subsection 2.6. A single step approach would reduce much of the uncertainty in the predicted ice jam surface profile, as the ice jam would not have to be subjected to excessive grounding, slumping and ice erosion. However, this was not possible due to various practical constraints such as climatic conditions and a lack of available personnel trained in the operation of the RPA.

4.2. Modelling

Even though the measured and modelled elevations and ice thicknesses are similar, some deviations are noted that result from difficulties modelling the 2022 Aux Saumons River ice jam. For one, HEC-RAS assumes that water always flows under the ice jam in Figure 8(b), where in reality there is clear evidence of grounded ice in the DEM (see section 3.1).

Thus, the modelled underflow is not completely realistic and ultimately introduces errors into the predicted ice surface profile and ice jam thicknesses; however, this assumption is unavoidable for the model to maintain continuity. Another possible explanation for the small deviations could be that HEC-RAS does model narrow ice jams. It is possible that the 2022 Aux Saumons River ice jam behaved more like a narrow ice jam rather than a wide-river ice jam as modelled. Narrow jams occur when, in addition to ice juxtaposing upstream of an ice cover, frazil flocs and pans also submerge under the ice cover and deposit on its underside (Lindenschmidt 2020). This phenomenon is not modelled in the equilibrium ice jam equation. Additionally, the fact that the HEC-RAS models were run in steady-state, whereas in reality the ice jam was highly transient, as noted by the fluctuations of discharge and water level in Figure 2, is bound to bring some uncertainty into the modelled results. Finally, HEC-RAS cannot account for ice erosion processes inducing changes to the predicted ice thickness profiles. Exploring other one-dimensional models (e.g. RIVICE and River1D) capable of modelling narrow ice jams, transient ice jam formation and ice erosion processes may provide more accurate predictions of the ice surface elevation and thickness profiles of the Aux Saumons River ice jam in 2022. Despite its limitations, HEC-RAS remains a simple to implement and widely used hydraulic model, and consequently exploring the potential of photogrammetry to calibrate HEC-RAS ice jam models is a useful exercise for researchers and practicing hydraulic engineers.

The requirement of 1D models to often force flow through a narrow area above the bed limits their ability to model ice jams containing grounded sections. Evidence of flow moving around grounded sections in the Aux Saumons ice jam is apparent by the contiguous region of lower elevations in the DEM of Figure 4(a). Also, large parts of this region turn to open water in the March 18 orthomosaic (Figure 4(d)), providing further support that the flow there caused thermal degradation of the ice jam in these locations as it flowed around the grounded sections between the time it set in place on February 21 to the March 18. Two-dimensional models such as CRISSP2D or the KHIONE module of Telemac-Mascaret may help overcome the limitations inherent to 1D ice modelling approaches when attempting to model flow through ice jams with grounded sections. However, to the authors' knowledge, modelling heavily grounded ice jams using a 2D numerical model has not yet been attempted and future research on this topic should prove beneficial.

5. CONCLUSIONS

RPA photogrammetry has been demonstrated to be a low-cost, rapidly deployable technique for gathering high-resolution spatial data of an ice jam for calibrating and validating a 1D numerical ice jam model. Inspecting the large-scale orthomosaics can reveal information about the ice jam's condition and how it formed, information that would otherwise go unnoticed on the ground. Longitudinal hinge fractures near the banks, showing where the ice jam sagged lower as the flood waters receded, or central cracks, indicating where the ice jam grounded near one bank, but sagged lower into the thalweg near the other bank, are two examples. Furthermore, frozen puddles of water visible in the flood plain provide useful information on the extents of overbank flooding during the formation of the ice jam. Moreover, photogrammetry DEMs can be used to extract continuous longitudinal elevation profiles of the ice jam's surface, allowing a numerical model's simulated ice profile to be validated. Finally, if grounded locations in the DEM can be identified and bathymetric measurements are available, estimates of ice jam thickness in these locations can possibly be obtained (using a similar approach to Alfredsen *et al.* 2018), thus providing additional calibration data to improve numerical modelling results.

The modelling of the 2022 Aux Saumons River ice jam highlighted an important limitation of one-dimensional numerical models such as HEC-RAS: they are unable to model grounded sections of the ice jam or the 2D channels that the flow follows to move around them. Rather, as the underside of the ice jam approaches the bed, the models maintain continuity by preventing the underside of the ice jam from descending all the way to the bed. This is unrealistic. However, because of the many advantages of 1D models (e.g. ease of use and speed), future development efforts to accommodate the effects of ice grounding would be beneficial to improve the versatility of these handy one-dimensional ice models. Alternatively, investigating the potential of two-dimensional fluvial ice models such as CRISSP2D or Telemac-Mascaret's KHIONE ice module to account for 2D flow around grounded sections of ice may produce a more accurate representation of the ice jam, yet at the cost of considerably greater computational requirements. Finally, regular RPA flights over the ice jam could provide temporal information on the ice jam's state and elevations, which could be used to validate transient simulations of the ice jam as it responds to recorded discharge measurements and its eventual release. In summary, our study has shown RPA photogrammetry to be a convenient remote sensing technique to supplement traditional *in situ* measurements to acquire data to development and calibrate numerical ice jam models.

ACKNOWLEDGEMENTS

DATA AVAILABILITY STATEMENT

All relevant data are included in the paper or its Supplementary Information.

CONFLICT OF INTEREST

The authors declare there is no conflict.

REFERENCES

Albadra, A., Wood, K., Berthoud, L., Calway, A., Watson, M., Thomas, H., Richardson, T., Liu, E. & Chigna, G. 2020 Determining the three-dimensional structure of a volcanic plume using Unoccupied Aerial System (UAS) imagery. *Journal of Volcanology and Geothermal Research* **407**, 106731.

Alfredsen, K., Haas, C., Tuhtan, J. A. & Zinke, P. 2018 Brief communication: mapping river ice using drones and structure from motion. *Cryosphere* **12.2**, 627–633.

Béland, M.-L. 2018 Un pont ferroviaire s'effondre à Sherbrooke. In: *Spectre Média 14/10/2018*.

Beltaos, S. 2018 The 2014 ice – jam flood of the Peace-Athabasca Delta: insights from numerical modelling. *Cold Regions Science and Technology* **155** (August), 367–380.

Beltaos, S. 2019 Numerical prediction of ice-jam profiles in lower Athabasca river. *Canadian Journal of Civil Engineering* **46** (8), 722–731.

Beltaos, S. & Burrell, B. C. 2010 Ice-jam model testing: Matapedia River case studies, 1994 and 1995. *Cold Regions Science and Technology* **60.1**, 29–39.

Beltaos, S. & Tang, P. 2013 Applying HEC-RAS to simulate river ice jams: snags and practical hints. In *CGU HS Committee on River Ice Processes and the Environment*, pp. 415–430.

Beltaos, S., Tang, P. & Rowsell, R. 2012 Ice jam modelling and field data collection for flood forecasting in the Saint John River, Canada. *Hydrological Processes* **26** (17), 2535–2545.

Bigdeli, B., Amini Amirkolaee, H. & Pahlavani, P. 2018 DTM extraction under forest canopy using LiDAR data and a modified invasive weed optimization algorithm. *Remote Sensing of Environment* **216** (July), 289–300.

Blackburn, J. & She, Y. 2019 A comprehensive public-domain river ice process model and its application to a complex natural river. *Cold Regions Science and Technology* **163** (July 2018), 44–58.

Carson, R., Beltaos, S., Groeneveld, J., Healy D., She Y., Malenchak, J., Morris, M., Saucet, J., Kolerski, T. & Shen, H. T. 2011 Comparative testing of numerical models of river ice jams. *Canadian Journal of Civil Engineering* **38** (6), 669–678.

Chu, T. & Lindenschmidt, K. E. 2016 Integration of space-borne and air-borne data in monitoring river ice processes in the Slave River, Canada. *Remote Sensing of Environment* **181**, 65–81.

Daly, S. & Vuyovich, C. 2003 Modeling river ice with HEC-RAS. In: *12th Workshop on River Ice Covered Rivers*, June 19–20, pp. 280–290.

Das, A. & Lindenschmidt, K. E. 2021 Evaluation of the implications of ice-jam flood mitigation measures. *Journal of Flood Risk Management* **14** (2), 1–15.

Das, A., Rokaya, P. & Lindenschmidt, K.-E. 2020 Ice-jam flood risk assessment and hazard mapping under future climate. *Journal of Water Resources Planning and Management* **146** (6), 04020029.

Das, A., Budhathoki, S. & Lindenschmidt, K.-E. 2022 A stochastic modelling approach to forecast real-time ice jam flood severity along the transborder (New Brunswick/Maine) Saint John River of North America. *Stochastic Environmental Research and Risk Assessment* 0123456789.

David, C. G., Kohl, N., Casella, E., Rovere, A., Ballesteros, P. & Schlurmann, T. 2021 Structure-from-Motion on shallow reefs and beaches: potential and limitations of consumer-grade drones to reconstruct topography and bathymetry. *Coral Reefs* **40.3**, 835–851.

Ehrman, J., Clark, S. & Wall, A. 2021 Ice roughness estimation via remotely piloted aircraft and photogrammetry. *Cryosphere* **15.8**, 4031–4046.

Ely, J. C., Graham, C., Barr, I. D., Rea, B. R., Spagnolo, M. & Evans, J. 2017 Using UAV acquired photography and structure from motion techniques for studying glacier landforms: application to the glacial flutes at Isfallsglaciären. *Earth Surface Processes and Landforms* **42. 6**, 877–888.

Engineers, U. A. C. of 2022 HEC-RAS User's Manual version 6.2. In.

Kalacska, M., Lucanus, O., Arroyo-Mora, J. P., Laliberté, É., Elmer, K., Leblanc, G. & Groves, A. 2020 Accuracy of 3d landscape reconstruction without ground control points using different uas platforms. *Drones* **4.2**, 1–26.

Lindenschmidt, K. E. 2017 RIVICE-A non-proprietary, open-source, one-dimensional river-ice model. *Water (Switzerland)* **9** (5).

Lindenschmidt, K.-E. 2020 *River Ice Processes and Ice Flood Forecasting*.

Lindenschmidt, K.-E. & Li, Z. 2018 Monitoring river ice cover development using the Freeman–Durden decomposition of quad-pol Radarsat-2 images. *Journal of Applied Remote Sensing* **12.02**, 1.

Lindenschmidt, K. E. & Rokaya, P. 2019 A stochastic hydraulic modelling approach to determining the probable maximum staging of Ice-Jam floods. *Journal of Environmental Informatics* **34** (1), 45–54.

Lindenschmidt, K. E., Sydor, M. & Carson, R. W. 2012 Modelling ice cover formation of a lake-river system with exceptionally high flows (Lake St. Martin and Dauphin River, Manitoba). *Cold Regions Science and Technology* **82**, 36–48.

Los, H. & Pawlowski, B. 2017 The use of Sentinel-1 imagery in the analysis of river ice phenomena on the lower Vistula in the 2015–2016 winter season. In *2017 Signal Processing Symposium, SPSympo 2017*, pp. 0–4.

Nezhikhovsky, R. A. 1964 Coefficients of roughness of bottom surface on slush-ice cover. *Soviet Hydrology* **2**, 127–150.

Rødtang, E., Alfredsen, K., . & Juárez, A. 2021 Drone surveying of volumetric ice growth in a steep river. Frontiers in Remote Sensing **2**, 1–11.

Rokaya, P., Wheater, H. & Lindenschmidt, K.-E. 2019 Promoting sustainable ice-jam flood management along the Peace River and Peace-Athabasca Delta. *Journal of Water Resources Planning and Management* **145** (1), 04018085.

Tracy, B. T. & Daly, S. F. 2003 River ice delineation with RADARSAT SAR. In *12th Workshop on the Hydraulics of Ice Covered Rivers*, p. 11.

Unterschultz, K. D., van der Sanden, J. & Hicks, F. E. 2009 Potential of RADARSAT-1 for the monitoring of river ice: results of a case study on the Athabasca River at Fort McMurray, Canada. *Cold Regions Science and Technology* **55.2**, 238–248.

Westoby, M. J., Brasington, J., Glasser, N. F., Hambrey, M. J. & Reynolds, J. M. 2012 Structure-from-Motion' photogrammetry: a low-cost, effective tool for geoscience applications. *Geomorphology* **179**, 300–314.

Williams, B. S., Das, A., Johnston, P., Luo, B. & Lindenschmidt, K. E. 2021 Measuring the skill of an operational ice jam flood forecasting system. *International Journal of Disaster Risk Reduction* **52**, 1–12.

Zhang, F., Li, Z. & Lindenschmidt, K. E. 2019 Potential of RADARSAT-2 to improve Ice thickness calculations in remote, poorly accessible areas: a case study on the Slave River, Canada. *Canadian Journal of Remote Sensing* **45** (2), 234–245.

Zufelt, J. E. 2005 Modeling ice jams using HEC-RAS: the three creeks project. In *CGU HS Committee on River Ice Processes and the Environment, 13th Workshop on the Hydraulics of Ice Covered Rivers*, Hanover, NH, United States, pp. 15–16.